الجمهورية الديمقراطية الشعبية الجزائرية

وزارة التعليم العالي والبحث العلمي

جامعة سعد دحلب بليدة

معهد الطيران والدراسات الفضائية

Presented for obtaining the Master degree in Space Telecommunication

By : Fatma-zohra Medina Guettouche

Subject

Moisture content retrieval from agricultural fields using Synthetic Aperture Radar polarimetry

Presented in front of the examination jury composed of :

Mme	MOUFFOK Lila	Professor	at IAES	President
Mr	AZMEDROUB Boussad	Professor	at IAES	Thesis Examiner

Under the supervision of:

Mr	TAHRAOUI Sofiane	Professor	at IAES

Abstract

In the past years, polarimetric Synthetic Aperture Radars have contributed in the achievement of great advances in remote sensing. Employing SAR polarimetry turned out to be very effective in diverse applications of several fields such as agriculture, detection, ecology…etc.

This work has for aim the retrieval of the soil moisture content from bare soils regions only, for this purpose Synthetic Aperture Radar have been exploited using their polarimetric properties. First, bare surface discrimination is applied using a new approach, and then the soil moisture content is estimated by applying an empiric inversion method.

This work is intended to the agricultural field, indeed harnessing this technique for watering agricultural lands would have amazing returns giving the fact that this technique would help spotting with exact measures the areas in need of more moisture, which would improve the growth of the sowings, and consequently, a positive outcome on water savings is reached.

نبذة

في الآونة الأخيرة، ساهمت الرادارات ذي الفتحة الاصطناعية في تحقيق تقدم مهم فيما يتعلق بالكشف عن بعد، تبين أن استعمال قياس الاستقطاب للرادارات ذي الفتحة الاصطناعية جد فعال في عدة تطبيقات لمختلف الميادين مثل الزراعة، الكشف، علم البيئة...الخ.

يهدف هذا العمل إلى استرداد محتوى الرطوبة من الحقول الزراعية مباشرة من التربة العارية، ولتحقيق ذلك، استغلت الخصائص الاستقطابية للرادار ذي الفتحة الاصطناعية. أولا، سيتم تمييز المساحة العارية عن غيرها وذلك بتطبيق تقنية جديدة، ثم نطبق طريقة إقلاب تجريبية لاسترداد محتوى الرطوبة.

هذا العمل مكرس أكثر للميدان الزراعي، في الواقع استعمال تلك التقنية لسقي الحقول الزراعية سيكون له نتائج جد مرضية وهذا راجع لدقة القياسات التي تحققها التقنية المعناة في تمييز المناطق التي تحتاج إلى ري أكثر، مما يؤدي إلى تحسين نمو المزروعات، وبالتالي سيحقق اقتصاد مصادر معتبر.

Résumé

Les dernières années, les Radars à Synthèse d'Ouverture ont contribué à l'achèvement d'importants progrès en ce qui concerne la détection à distance. Employant la polarimétrie des Radars à Synthèse d'Ouverture s'est avéré être très efficace pour divers applications de plusieurs domaines comme l'agriculture, la détection, l'écologie...etc.

Ce travail a pour but la récupération du contenu en humidité dans les régions à sols nus seulement, afin de le réaliser, les propriétés polarimétriques du Radar à Synthèse d'Ouverture sont exploitées. D'abord, une discrimination de surfaces nues est appliquée en utilisant une nouvelle méthode, ensuite, la teneur en humidité est récupérée en appliquant une méthode empirique d'inversion.

Ce travail est beaucoup plus destiné au domaine d'agriculture, en effet, l'utilisation de cette technique pour l'arrosage des champs agricoles pourrait avoir d'incroyables retours donnant le fait que cette technique pourrait détecter avec d'exactes mesures les régions faiblement humides, ce qui pourrait améliorer la croissance des plants, par conséquent, des économies de ressources assez considérables seront abouties.

Acknowledgements

First and foremost, I am thankful to God, the most gracious most merciful for helping me finishing this modest work.

I am infinitely grateful to my family members, particularly my parents for their patience and continuous encouragements and belief in me throughout my whole life, to my brothers for being always my source of strength, and to my nephews and niece for bringing me daily joy.

I would like to express my gratitude to my supervisor Pr S. TAHRAOUI for his patience, support and guidance. It has been an honor to work under his supervision.

I extend my thanks to Mr B. AZMEDROUB for his help.

I thank all the teachers from Primary School until now, whom without I would not be here.

At last but not least, I would like to thank my friends for their accompany through this journey.

Content

Acronyms

SAR	Synthetic Aperture Radar
X-BRAGG	Extended BRAGG
BSA	Back Scatter Alignment
RGB	Red-Green-Blue
PolSAR	Polarimetric Synthetic Aperture Radar
SR	Surface scattering
VD	Volume scattering
DB	Double-Bounce scattering
MC	Moisture Content

List of figures

List of tables

Introduction

The study and the exploitation of the characteristics of the electromagnetic field such as polarization and frequency, as well as the study of its interactions and phenomena associated with backscattered energy in several combinations of these characteristics (frequency and polarization), over the past decades, has led to tremendous advances in the theory of electromagnetic wave polarimetry resulting in the theory of radar polarimetry, and with technological advancement and the development of high resolution radar devices, radar polarimetry has experienced increasingly practical areas of application.

Synthetic Aperture Radar (SAR) systems are active sensors for earth observation; they are more efficient than optical sensors due to their independence from daylight and meteorological conditions. SAR images acquisition is based on the emission of electromagnetic waves and the storage of the target echoes (backscattered waves), the information within those last depends on the wavelength, the polarization state of the wave, the roughness and the dielectric constant of the ground.

The SAR systems operate in microwaves, there is two types: airborne and spaceborne sensors, they can operate in mono-polarization or multi-polarization modes, we have to denote that the mono-polarized radars are limited for mapping natural surfaces, whereas multi-polarized one are able to acquire more information about the target shape and geometry, in addition to some physical parameters of the natural environment such as forest's height, density and soil moisture.

As aforementioned, the polarization information contained in the backscattered waves are related to the geometrical structure of the target, its reflectivity, shape and orientation, as well as its geophysical properties such as humidity, roughness…etc. This had opened the door to several SAR polarimetry applications in different fields [1]:

- Forest vegetation: the discrimination of forest's height, biomass and structure, and the surveillance of the canopy extinction…etc.
- Agriculture: the extraction of the soil moisture content, and the discrimination of soil roughness…etc.
- Urban monitoring: the determination of geometric and dielectric properties.
- Ecosystem change surveillance.

SAR polarimetry is employed to extract soil moisture content from bare soils, this estimation has been under investigation in the last decade, and satisfactory results have been achieved using new model-based decompositions (Bragg and extended Bragg "X-Bragg" scattering models).

In this study, a new extended Bragg scattering-based methodology will be used for bare soil detection, it is based on the exploitation of special structures of the coherency matrix assumed for X-Bragg scattering, simulated and operational data are used. [11]

In the following, the content of the chapters is illustrated:

1. Chapter one will introduce an overview of polarimetric synthetic aperture radar (SAR), adducing fundamental electromagnetic wave polarimetry.

2. Chapter two will present the approaches employed for targets decomposition and classification, and for surface discrimination.

3. Chapter three will be dedicated to the study of simulated data and operational sensors data.

CHAPTER

1

Principles of PolSAR

1.1 Introduction

The RADAR (**Ra**dio **D**etection **A**nd **R**anging), was developed for the detection of ships and aircrafts in the 20's. It has been widely used for Earth observation and imaging for more than 40 years. A huge forward step has been taken in this field since the great advances in space science and technologies over the last decade.

Synthetic aperture radar (SAR) operates in microwave and uses a wide band of frequencies, this allows the radar to be independent from solar light and meteorological conditions (i.e. the radar can take images anytime no matter the weather). The SAR systems are able to acquire images using mono-polarization or multi-polarization channels, the difference between the two is in the amount of information extracted from each of them, indeed multi-polarized SAR gives more information about the illuminated area.

In the following, we will present more about SAR systems basics more precisely polarimetric SAR systems.

1.2 Synthetic Aperture Radar

The Synthetic-aperture radar "SAR" is a form of moving radar that uses a side-looking acquisition. While the sensor is moving (within satellites or planes), it transmits signal, and receives the related backscattering from the illuminated area.

As aforementioned, the SAR imaging system is mounted on a moving platform, which is situated at a height H, and moves with a velocity "VSAR". The antenna is directed perpendicularly to the flight direction (the Azimuth), and radiate toward the ground with a look angle θ_0. **Fig 1.1** illustrates the SAR imaging geometry [2].

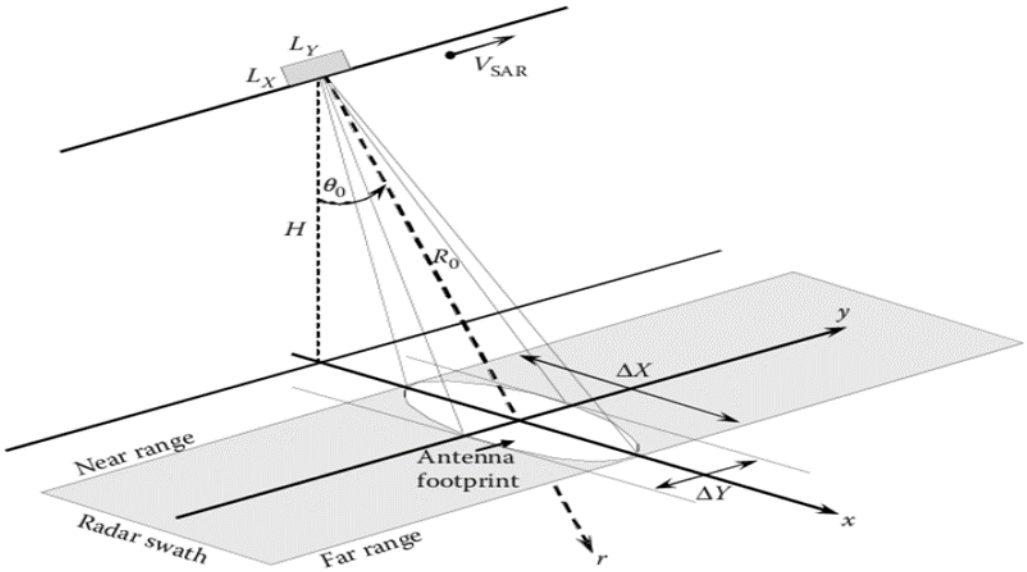

Fig 1.1 SAR imaging geometry

Where:

- *r* is the radial axis (range).
- *Antenna footprint* is the area covered by the antenna beam.
- *Radar swath* is the area scanned by the antenna beam.

1.2.1 SAR spatial resolution

Radar resolution is an essential parameter; it is defined as the ability to distinguish between two targets in azimuth and in range.

The range resolution depends on the duration of the transmitted pulse bandwidth B; it is given by the following equation [2]:

$$\delta r = \frac{C}{2B} \qquad (1.1)$$

Where C is light celerity.

Due to the radar motion, the SAR azimuth resolution is quite high, the cause is very simple, since the transmission and the reception occur at different times the radar sensor will be at different positions, and by means of signal processing a virtual aperture is constructed which is much wider than the real one (this is why the term synthetic aperture is used); the SAR azimuth resolution is expressed as follows: [2]

$$\delta y = \frac{Ly}{2} \qquad (1.2)$$

1.2.2 Basics of SAR system

Like any radar the SAR works like an optical radar, the typical system consists of a transmitter, a switch, an antenna, a receiver, a data recorder and a processor.
The transmitter generates pulsed electromagnetic waves; the switch directs them to the antenna, which transmits them to the scanned area. Then, it collects the related backscattering. These last are converted to digital data by the receiver and are stored in the data recorder for later processing and display. **Fig 1.2** below shows a basic radar system. [3]

.

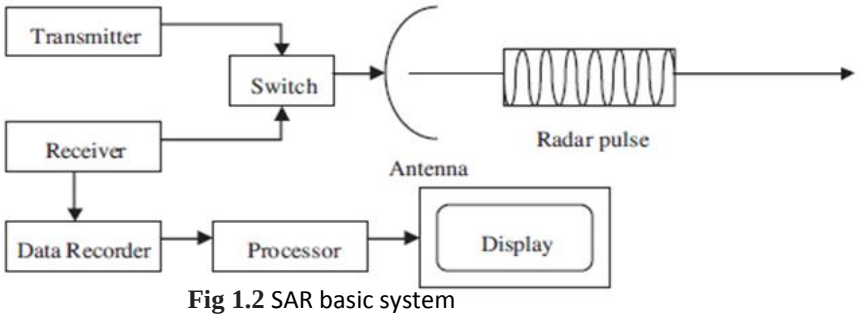

Fig 1.2 SAR basic system

1.2.3 Sar image formation

As mentioned earlier, the SAR antenna transmits pulsed waves to the target and stores the target echoes along the synthesized antenna.

The stored echoes forms a two dimensional matrix called raw data; two different scanning methods are used to form each pixel of the matrix, a detailed explanation about each process can be found in [8]. We must denote that the SAR image is complex, the amplitude and the phase information are directly associated to the reflectivity of all the scatterers contained in the SAR resolution cell [3].

Fig 1.3 below summarizes the SAR image processing highlighting two major tasks:

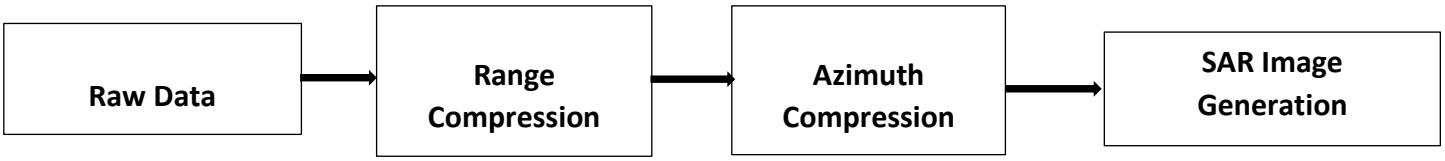

Fig 1.3 basic scheme for SAR image formation

1.2.4 SAR image speckle

SAR image speckle is a disturbing noise, which degrades the data within and affects the accuracy of their processing; it is originated from the coherent summation of each individual scatterer.

In order to reduce the effect of the speckle two solutions might be used. The first one is a multi-look incoherent averaging that performs an incoherent sum of the amplitudes or the intensity of images accordingly to the azimuthal direction, though, the speckle will be significantly reduced and the spatial resolution will be degraded. The second approach is using adaptive filters, these last perform a smoothing in the homogeneous regions without blurring the structures in the image, and many adaptive filters have been

Proposed amongst them: Lee, Frost, Gamma-Gamma MAP… etc. in this work Lee filter will be used.

1.3 Radar polarimetry

Radar polarimetry (the measure of the polarization) deals with the vector nature of a polarized electromagnetic wave. It is the science of acquiring, processing and analyzing the polarization state of an electromagnetic field.
In order to describe the preceding process, let define the wave polarization in the following.

1.3.1 Propagation of a monochromatic plane electromagnetic wave

A monochromatic plane wave refers to a single frequency/wavelength electromagnetic wave, which travels in space, contrarily to sunlight it is one color only. From Maxwell's equations and for a special case (where the monochromatic wave has a constant amplitude and the medium of propagation is linear and free of charges), the electric field can be written as [4]:

$$\vec{E}(\vec{r},t) = R\left(\underline{\vec{E}}(\vec{r}) e^{j\omega t} \right) \qquad (1.3)$$

The propagation of an electromagnetic wave is ruled by the propagation equation defined as follows [4]:

$$\Delta \underline{\vec{E}}(\vec{r}) + \omega^2 \mu\varepsilon \left(1 - j\frac{\sigma}{\varepsilon\omega} \right) \underline{\vec{E}}(\vec{r}) = \Delta \underline{\vec{E}}(\vec{r}) + \underline{k}^2 \, \underline{\vec{E}}(\vec{r}) = 0 \qquad (1.4)$$

With :

$$\underline{k} = \frac{\omega}{v} \sqrt{1 - j\frac{\sigma}{\varepsilon\omega}}$$

We may represent the electric field in an orthonormal basis (x, y, z), where the direction of the propagation k = z, its expression becomes [4]:

$$\underline{\vec{E}}(z) = \underline{\vec{E}_0} e^{-\alpha z} e^{-j\beta z} \quad (1.5)$$

With : $$\underline{E_{0z}} = 0$$

Where β stands for the wave number in time domain, whereas α represent an attenuation factor. In the vectorial form and back to time domain, the prior expression becomes [4]:

$$\vec{E}(z,t) = \begin{bmatrix} E_{0x}\, e^{-\alpha z} \cos(\omega t - kz + \delta_x) \\ E_{0y}\, e^{-\alpha z} \cos(\omega t - kz + \delta_y) \\ 0 \end{bmatrix} \quad (1.6)$$

1.3.2 Polarization ellipse

The spatial evolution of a plane monochromatic wave follows a helicoidal trajectory along the z-axis; the analysis of this evolution in time domain is observed at a fixed position z = z_0.

After studying the temporal behavior of the wave, we may point out that the wave's propagation describes a characteristic ellipse which equation's is defined as follow [4]:

$$\left(\frac{E_x(z_0,t)}{E_{0x}}\right)^2 - 2\frac{E_x(z_0,t)E_y(z_0,t)}{E_{0x}E_{0y}}\cos(\delta_y - \delta_x) + \left(\frac{E_y(z_0,t)}{E_{0y}}\right)^2 = \sin(\delta_y - \delta_x) \quad (1.7)$$

The so-called polarization ellipse describes the wave polarization; its shape is determined by three parameters shown in the subsequent figure [4]:

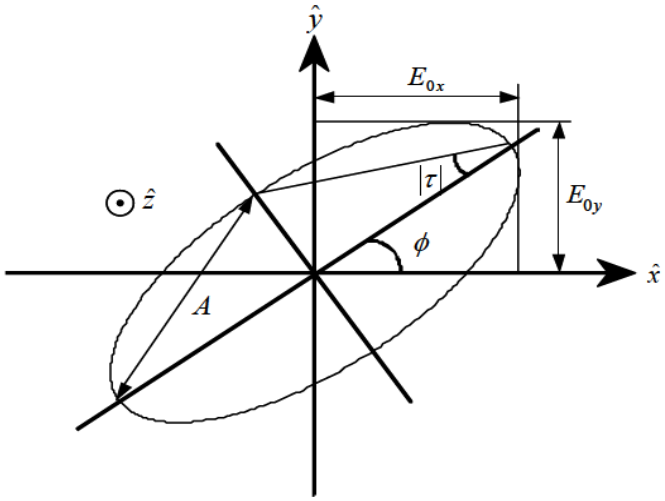

Fig 1.4 The polarization ellipse

Where:

- A is the ellipse amplitude : $$A = \sqrt{E_{0x}^2 + E_{0y}^2} \quad (1.8)$$
- φ is the ellipse orientation (the angle between the ellipse major axis and x-axis):

$$\tan 2\emptyset = 2\frac{E_{0x}E_{0y}}{E_{0x}^2 - E_{0y}^2}\cos(\delta_y - \delta_x) \quad (1.9)$$

- /τ/ is the ellipse aperture (ellipticity):

$$|\sin 2\tau| = 2\frac{E_{0x}E_{0y}}{E_{0x}^2 + E_{0y}^2}|\sin\delta| \quad (1.10)$$

1.3.3 Jones vector

The representation of a plane monochromatic electric field under the form of a Jones vector aims to describe the wave polarization using the minimum amount of information; it contains complete information about the amplitudes and the phases of the electric field vectors. The vectorial form of a Jones vector is defined as follow [4]:

$$\underline{E} = \begin{bmatrix} E_{0x}e^{j\delta_x} \\ E_{0y}e^{j\delta_y} \end{bmatrix} \quad (1.11)$$

The definitions of the polarization determined from the polarization ellipse or a Jones vector are equivalent; therefore, the Jones vector can be written under a more effective form, where it is a function of the characteristics of the polarization ellipse [4]:

$$\underline{E} = Ae^{j\alpha}\begin{bmatrix}\cos\emptyset & -\sin\emptyset\\ \sin\emptyset & \cos\emptyset\end{bmatrix} \qquad (1.12)$$

1.3.4 Polarization ratio

The polarization ratio ρ is another efficient way to determine the polarization of a monochromatic wave; it is defined as [4]:

$$\rho = \frac{\underline{E_y}}{\underline{E_x}} = \frac{E_{0y}}{E_{0x}}\, e^{j(\delta_y - \delta_x)} \qquad (1.13)$$

It can also be written as a function of the characteristics of the polarization ellipse:

$$\rho = \frac{\sin\emptyset\cos\tau + j\ \cos\emptyset\sin\tau}{\cos\emptyset\cos\tau - j\ \sin\emptyset\sin\tau} \qquad (1.14)$$

The table below summarizes all the canonical polarization states of a monochromatic plane electromagnetic wave in function of the polarization ellipse, Jones vector and the polarization ratio [4].

Polarization States	Unitary Jones vector	Orientation $\emptyset$	Ellipticity τ	Polarization ratio
Horizontal (H)	$\begin{bmatrix}1\\0\end{bmatrix}$	0	0	0
Vertical (V)	$\begin{bmatrix}0\\1\end{bmatrix}$	$\frac{\pi}{2}$	0	∞
Linear +45°	$\frac{1}{\sqrt{2}}\begin{bmatrix}1\\1\end{bmatrix}$	$\frac{\pi}{4}$	0	1
Linear -45°	$\frac{1}{\sqrt{2}}\begin{bmatrix}-1\\1\end{bmatrix}$	$\frac{3\pi}{4}$	0	-1
Left circular	$\frac{1}{\sqrt{2}}\begin{bmatrix}1\\j\end{bmatrix}$	None	$\frac{\pi}{4}$	j
Right circular	$\frac{1}{\sqrt{2}}\begin{bmatrix}1\\-j\end{bmatrix}$	None	$-\frac{\pi}{4}$	-j

Table 1.1 Canonical polarization states

After introducing electromagnetic wave and how to describe its polarization by the mean of the Jones vector, we will describe in the following the mainstay notion of polarimetry, the scattering matrix.

1.3.5 Scattering matrix

An electromagnetic wave travels in time and space, along this voyage, the wave may interact with a certain target, consequently, the target absorbs a part of the energy carried by the incident wave, whilst, the other part is reradiated as a new electromagnetic wave, which has different properties from the incident one.

The purpose is to employ these changes to identify the target. The figure **Fig 1.5** illustrates the interaction of an electromagnetic wave with a target. [2]

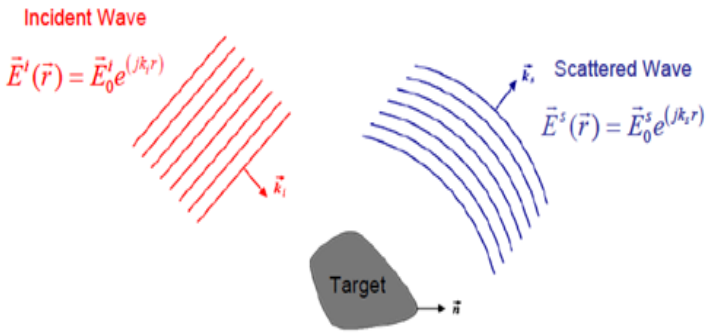

Fig 1.5 The interaction of an electromagnetic wave with a target

In order to exploit the vectorial nature of the polarized electromagnetic waves, we will express the scattering process occurring at the target as a function of the Jones vectors of the incident and the scattered fields, and a specific matrix called the "scattering matrix", as follows [2]:

$$\underline{E^S} = \frac{e^{-jkr}}{r}\left[S_{(\perp,\parallel)}\right]\underline{E^i} = \frac{e^{-jkr}}{r}\begin{bmatrix} S_{\perp\perp} & S_{\perp\parallel} \\ S_{\parallel\perp} & S_{\parallel\parallel} \end{bmatrix}\underline{E^i} \qquad (1.15)$$

When working with BSA convention (Backscattering configuration, which means that the transmitting and the receiving antennas are the same), an important property called "reciprocity" occurs, in this case, the scattering matrix is defined as [2]:

$$S_{(\perp,\parallel)} = \begin{bmatrix} S_{\perp\perp} & S_{\perp\parallel} \\ S_{\parallel\perp} & S_{\parallel\parallel} \end{bmatrix} \quad (1.16)$$

1.3.6 Coherency and covariance matrices

In order to have a more precise analysis of the radar target, we will introduce the concept of space and time travel varying stochastic processes, in which the target can be described by the second order moments of fluctuation, which will be extracted from the polarimetric coherency or covariance matrices, defined here below as [2]:

- The coherency matrix:

$$T_3 = \frac{1}{2}\begin{bmatrix} \langle|S_{HH} + S_{VV}|^2\rangle & \langle(S_{HH} + S_{VV})(S_{HH} - S_{VV})*\rangle & 2\langle(S_{HH} + S_{VV})S_{HV}^*\rangle \\ \langle(S_{HH} - S_{VV})(S_{HH} + S_{VV})^*\rangle & \langle|S_{HH} - S_{VV}|^2\rangle & 2\langle(S_{HH} - S_{VV})S_{HV}^*\rangle \\ 2\langle(S_{HH} + S_{VV})^* S_{HV}\rangle & 2\langle(S_{HH} - S_{VV})^* S_{HV}\rangle & 4\langle|S_{HV}|^2\rangle \end{bmatrix} \quad (1.17)$$

- The covariance matrix:

$$C_3 = \begin{bmatrix} \langle|S_{HH}|^2\rangle & \sqrt{2}\,\langle S_{HH}\, S_{HV}{}^*\rangle & \langle S_{HH}\, S_{VV}^*\rangle \\ \sqrt{2}\langle S_{HV} S_{HH}{}^*\rangle & 2\langle|S_{HV}|^2\rangle & \sqrt{2}\langle S_{HV} S_{VV}{}^*\rangle \\ \langle S_{VV} S_{HH}^*\rangle & \sqrt{2}\langle S_{VV} S_{HV}{}^*\rangle & \langle|S_{VV}|^2\rangle \end{bmatrix} \quad (1.18)$$

Where < > stands for the temporal or spatial averaging assuming ergodicity.

1.4 Lexicographic color-coded representation

The color-coded representation provides two alternatives to represent the information provided by the scattering image in a single image. There is many types of color codes; we will briefly explain the RGB color-coding.

In this particular color-code, we will combine the three primary colors (red, green and blue) to create new additive colors. Therefore, we can consider color as a three dimensional space as it is represented in the next figure [4]:

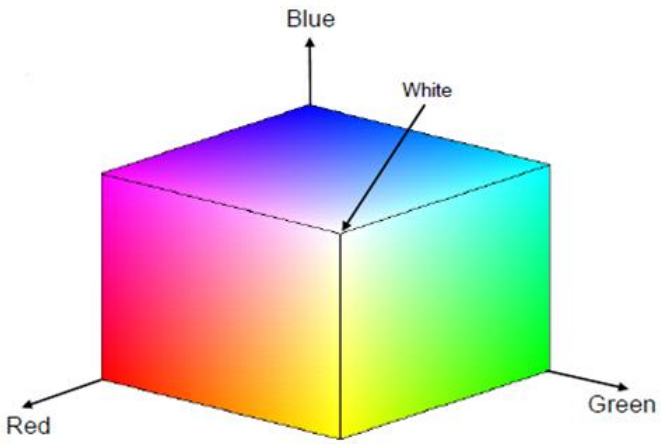

Fig 1.6 RGB color cube

To represent polarimetric information, the RGB color-code representation considers as dimensions of the color space the intensities of the scattering matrix elements, an example for a color codification is given below:

$$|S_{VV}{}^2| \ : \ \text{Red}$$

$$2|S_{HV}{}^2| \ : \ \text{Green}$$

$$|S_{HH}{}^2| \ : \ \text{Blue}$$

1.5 Conclusion

In this chapter, we have presented brief definitions and basics of the polarimetric SAR, in the next chapter we will present SAR images processing, and we will introduce the SAR polarimetric decompositions and classifications in order to characterize the nature of the covered area.

CHAPTER

2

Polarimetric data decompositions and classifications

2.1 Introduction

The data acquired from PolSAR images are directly related to the physical properties of the illuminated area, thus the identification of these properties are a necessity for numerous process. As the scattering process is a mixture of different scattering mechanisms, a decomposition of these different components is needed in order to get the most accurate representations of the information within the SAR image. Polarimetric decompositions provide a measure of the relative contributions of backscatter from different scattering mechanisms; multiple models of polarimetric decompositions have been proposed englobing coherent and incoherent targets [2].

Polarimetric classifications have for aim to categorize each cell pixel of a SAR image in a main scattering class, it's based on the target backscattering properties. Implementing target's decomposition is the main lead in order to extract classification features.

In the following, we shall introduce some of the PolSAR decomposition and classification methods. Furthermore, and as a brief introduction for this thesis goal, two model-based decompositions employed for surface discrimination will be defined.

2.2 Polarimetric SAR data decompositions

Due to the speckle noise and the random scattering vectors, radar remote sensing uses a statistical approach in order to describe targets by decomposing them using different decomposition's algorithms. Two main target decompositions have been proposed, which are:

2.2.1 Coherent decompositions

The aim of the coherent decomposition is to express the response of a given target which is very complex to study, as the combination of elementary mechanisms of coherent (canonical) scattereres, consequently the scattering matrix is presented as follows [4]:

$$[S] = \sum_{i=1}^{k} C_i \, [S]_i \qquad (2.1)$$

Where:

- S_i represents the scattering matrices of an independent scattering component in the same resolution cell.
- C_i is the weight of each matrix S_i in the combination leading to S.

A coherent component is also known as a pure object or a point scatterer, where the incident and the scattered waves are completely polarized waves.
There exist infinite algorithms using this type of decomposition. However, they are not all convenient to interpret the information contained in the matrix of the target. The most used ones are the Pauli decomposition, the Krogager decomposition, and the Cameron decompositions; we will briefly describe two decomposition methods in what follows.

2.2.1.1 Pauli decomposition

The Pauli decompositions a set of three 2*2 matrixes summed together to get the scattering matrix [4]:

$$[S] = \begin{bmatrix} S_{\perp\perp} & S_{\perp\parallel} \\ S_{\parallel\perp} & S_{\parallel\parallel} \end{bmatrix} = \alpha[S]_a + \beta[S]_b + \gamma[S]_c \qquad (2.2)$$

With:

$$[S]_a = \frac{1}{\sqrt{2}}\begin{bmatrix}1 & 0\\ 0 & 1\end{bmatrix},\ [S]_b = \frac{1}{\sqrt{2}}\begin{bmatrix}1 & 0\\ 0 & -1\end{bmatrix},\ [S]_a = \frac{1}{\sqrt{2}}\begin{bmatrix}0 & 1\\ 1 & 0\end{bmatrix} \quad (2.3)$$

$$\alpha = \frac{S_{\perp\perp} + S_{\perp\perp}}{\sqrt{2}},\ \beta = \frac{S_{\perp\perp} - S_{\perp\perp}}{\sqrt{2}},\ \gamma = \sqrt{2}S_{\perp\parallel} \quad (2.4)$$

- S_a represents the scattering matrix of a sphere, which is referred to single- or odd-bounce scattering, and α^2 determine the power scattered by targets characterized by single- or odd-bounce.

- S_b represents the scattering matrix of a dihedral oriented at 0°, which indicates a scattering mechanism characterized by double- or even-bounce, and β^2 represents the scattered power by this type of targets.

- S_c represents the scattering matrix of a diplane oriented at 45°, which is referred to dipole-like scattering. One of the best examples of this type of scattering is the volume scattering produced by the forest canopy.

The next figure shows an example of the Pauli decomposition applied on California Bay [4].

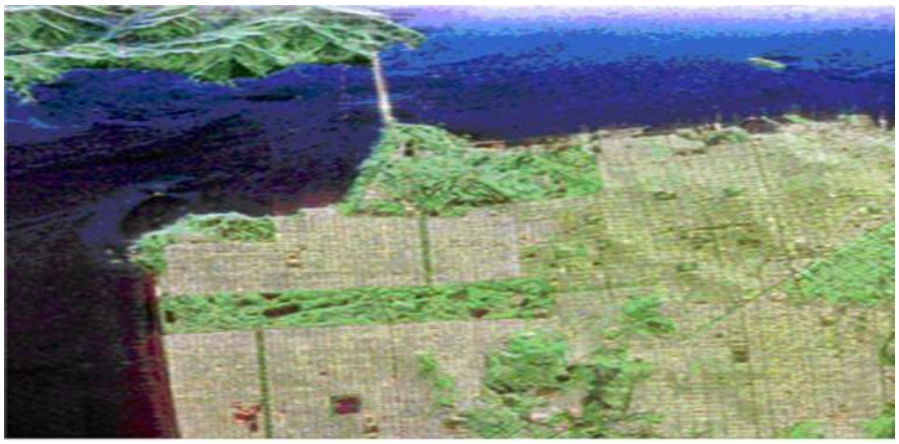

Fig 2.1 RGB

2.2.1.2 Krogager decomposition

The Krogager decomposition consists in factorizing the scattering matrix as the combination of the responses of a sphere, diplane and helix (the last two have an orientation angle of θ). The Krogager decompositions is defined in the following formula [4]:

$$\begin{aligned}\left[S_{(\perp,\parallel)}\right] &= e^{j\varphi}\left\{e^{j\varphi_s}\, k_s\, [S]_s + k_d\, [S]_d + k_h\, [S]_h\right\} \\ &= e^{j\varphi}\left\{e^{j\varphi_s}\, k_s \begin{bmatrix}1 & 0\\ 0 & 1\end{bmatrix} + k_d \begin{bmatrix}\cos 2\theta & \sin 2\theta\\ \sin 2\theta & -\cos 2\theta\end{bmatrix} k_h\, e^{\pm j2\theta} \begin{bmatrix}1 & \pm j\\ \pm j & 1\end{bmatrix}\right\}\end{aligned} \quad (2.5)$$

φ_s and φ are respectively the displacement of the sphere with respect to the diplane and the helix components, and the absolute phase.

- K_S, K_d and K_h are respectively the power scattered by the sphere-like component, the diplane-like component and the helix-like component.

The following figure shows an example of the Krogager decomposition applied on the same previous area [4].

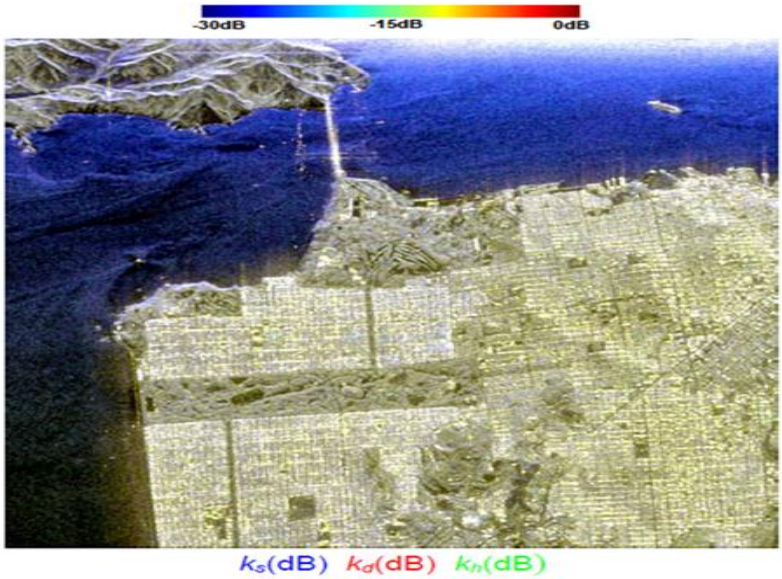

Fig 2.2 RGB color-coded image of the Krogager decomposition of California Bay

2.2.2 Incoherent decomposition

As the case of the coherent decomposition, incoherent decomposition considers the interaction as a result of elementary effects, but the sum is still incoherent and is conducted using the coherency matrix or the covariance matrix rather than the electric fields, each matrix will be decomposed as follows [4]:

$$\langle [C_3] \rangle = \sum_{i=1}^{k} p_i \, [C_3]_i \tag{2.6}$$

$$\langle [T_3] \rangle = \sum_{i=1}^{k} q_i \, [T_3]_i \tag{2.7}$$

There are many incoherent decompositions among them the model-based Freeman decomposition [4], the Hyunen decomposition [4], and the Eigenvector/Eigenvalue decomposition [4].

We will describe in the following the Eigenvector/Eigenvalue decomposition.

2.2.2.1 Eigenvector/Eigenvalue decomposition

The eigenvector/eigenvalue decomposition is based on the Eigen decomposition of the coherency matrix defined as following [4]:

$$\langle [T_3] \rangle = [U_3][\Sigma_3][U_3]^{-1} \tag{2.8}$$

Where:

- $[\sum_3]$ is a 3*3 real diagonal matrix which contains the eigenvalues of the coherency matrix [4]:

$$[\Sigma_3] = \begin{bmatrix} \lambda_1 & 0 & 0 \\ 0 & \lambda_2 & 0 \\ 0 & 0 & \lambda_3 \end{bmatrix} \tag{2.9}$$

- $[U_3]$ is a 3*3 unitary matrix which contains the eigenvector [4]:

$$[U_3] = \begin{bmatrix} \underline{u}_1 & \underline{u}_2 & \underline{u}_3 \end{bmatrix}$$

The eigenvectors are expressed as follows [4]:

$$\underline{u}_i = \begin{bmatrix} \cos\alpha_i & \sin\alpha_i \cos\beta_i e^{j\delta_i} & sin\,\alpha_i\, cos\,\beta_i e^{j\gamma_i} \end{bmatrix}^T \quad (2.10)$$

Then:

$$\langle [T_3] \rangle = \sum_{j=1}^{3} \lambda_i \, \underline{u}_i \underline{u}_i^{*T} \quad (2.11)$$

There are other parameters of the eigenvector-eigenvalue decomposition considered as secondary one they are listed here below [4]:

✓ The entropy: $H = -\sum_{i=1}^{3} p_i \, log_3(p_i) \quad with \; p_i = \frac{\lambda_i}{\sum_{k=1}^{3} \lambda_k}$ (2.12)

✓ The anisotropy: $A = \frac{\lambda_2 - \lambda_3}{\lambda_2 + \lambda_3}$ (2.13)

✓ The mean scattering angle alpha: $\underline{\alpha} = \sum_{i=1}^{3} p_i \alpha_i$ (2.14)

In order order to interpret the scattering mechanism giving by the eigenvector decomposition, we define a mean dominant mechanism as follows [4]:

$$\underline{u}_0 = \sqrt{\underline{\lambda}} \begin{bmatrix} cos\,\underline{\alpha} & sin\,\underline{\alpha}\, cos\,\underline{\beta}\, e^{j\underline{\delta}} & sin\,\underline{\alpha}\, cos\,\underline{\beta}\, e^{j\underline{\gamma}} \end{bmatrix}^T \quad (2.15)$$

With:

$$\underline{\beta} = \sum_{i=1}^{3} p_i \beta_i \qquad \underline{\delta} = \sum_{i=1}^{3} p_i \delta_i \qquad \underline{\gamma} = \sum_{i=1}^{3} p_i \gamma_i$$

The figure below represents a main scattering mechanism provided by the eigenvectors-eigenvalues decomposition [4]:

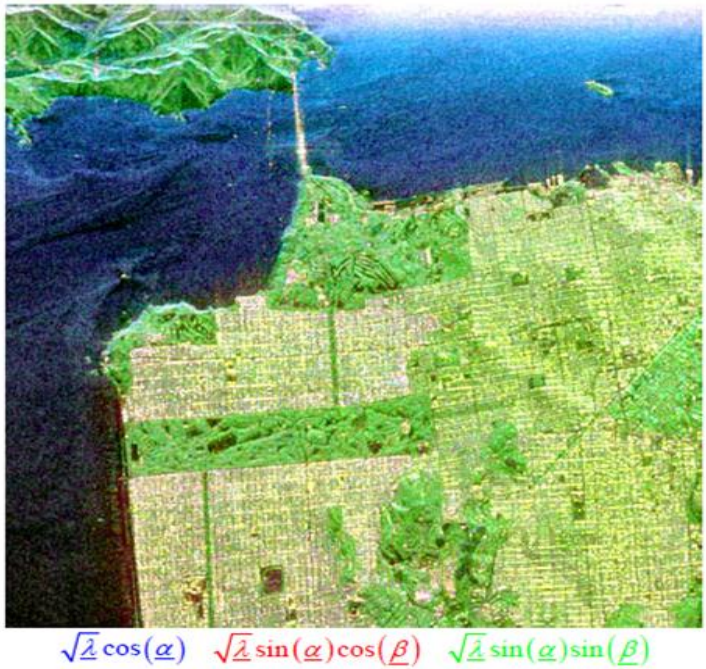

Fig 2.3 RGB color-coded of the Eigenvector-Eigenvalue decomposition of California Bay

2.3 Polarimetric SAR data classification

After decomposing the SAR targets, an interpretation of the decomposition's results must be done in order to identify polarimetric scattering mechanisms; this procedure is defined as SAR data classification. Multiple algorithms are proposed, some are based on direct classification [2] and other are based on statistical supervised or unsupervised segmentations (these last permits to assign each pixel of the SAR image to different scattering mechanisms using a minimum distance decision), in the following we shall only describe the H-A-α classification [4].

To classify SAR data without any supervision, Cloude and Pottier have proposed an algorithm based on the H/α decomposition, its main idea is to:

- Use the entropy "H" to measure the native reversibility of the scattering data.
- Use alpha "α" ti identify the underlying average scattering mechanisms.

To discriminate the different changes that occur to the signal wave (surface scattering (SR), volume scattering (VD) and double-bounce scattering (DB)), different class boundaries have been determined along the alpha axis and according to the low, medium and high degree of randomness along the entropy axes.

The following figure summarizes different canonical scattering mechanisms based on the H/α decomposition [2].

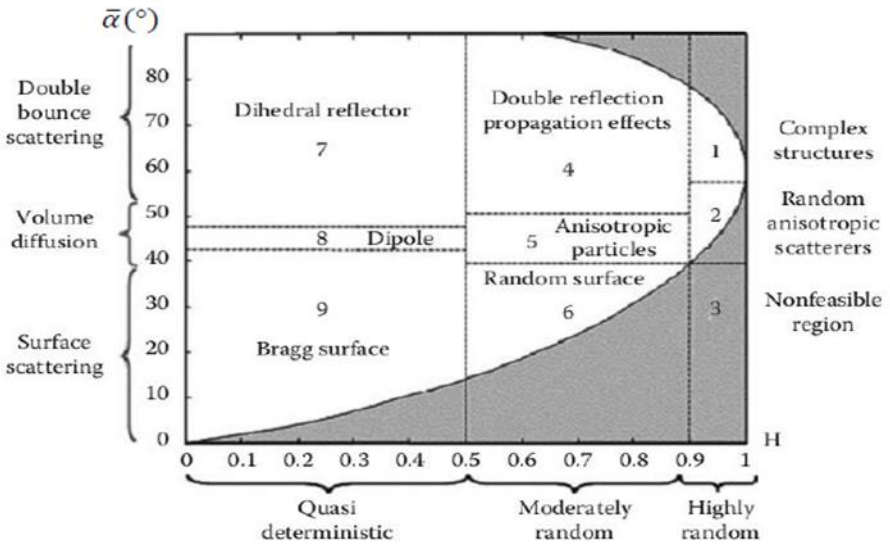

Fig 2.4 H/α characteristic plane

2.4 Surface discrimination

The goal of this thesis is to retrieve soil moisture information from agricultural lands. For this aim, rough surface discrimination from other contributions (vegetation, stones…) must be applied before the retrieval operation given the fact that additive components will compromise the accuracy of the process. In the following, we will explain briefly two model-based decompositions for surface description.

2.4.1 The Three-Components decomposition

The Three-Component decomposition is a model-based decomposition used to fit and to interpret SAR data, it has been proposed by Freeman and Durden. This model decomposes the measured coherency matrix into the sum of a BRAGG scattering component, a dihedral reflection (double bounce scattering) and a volume of randomly oriented dipoles [5].

2.4.1.1 The BRAGG scattering

The BRAGG scattering is a simple model approximation, it is quite a good choice for surface-scatter modeling, due to its robustness and parametrization simplicity (indeed, we only need to determine two parameters to describe the surface scattering) [5].

The corresponding scattering matrix is formulated as [5]:

$$S_B = m_s \begin{bmatrix} R_h(\theta, \varepsilon_s) & 0 \\ 0 & R_v(\theta, \varepsilon_s) \end{bmatrix} \qquad (2.16)$$

Where R_h and R_v are the horizontal and the vertical scattering coefficients, they depend on the incidence angle θ and the dielectric constant ε_s of the surface under study:

$$R_h := \frac{\cos\theta - \sqrt{\varepsilon_s - sin^2\theta}}{cos\,\theta + \sqrt{\varepsilon_s - sin^2\theta}}$$

$$R_h := \frac{(\varepsilon_s - 1)(sin^2\theta - \varepsilon_s(1 + sin^2\theta))}{(\varepsilon_s cos\,\theta + \sqrt{\varepsilon_s - sin^2\theta})^2} \quad (2.17)$$

The coherency matrix is [5]:

$$T_B = f_s \begin{bmatrix} 1 & \beta^* & 0 \\ \beta & |\beta|^2 & 0 \\ 0 & 0 & 0 \end{bmatrix} \quad (2.18)$$

With f_s the power contribution of the BRAGG scattering and β its scattering ratio:

$$f_s = \frac{m_s^2}{2} |R_h + R_v|^2 \quad , \quad \beta = \frac{R_h - R_v}{R_h + R_v} \quad (2.19)$$

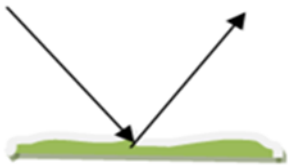

Fig 2.5 Surface (Bragg) scattering

2.4.1.2 The Double-Bounce scattering

The Double-Bounce scattering means a double reflection. One of the best examples of this type of scattering is the double reflection from building in urban areas. The corresponding scattering matrix and the coherency matrix are giving by [5]:

$$S_{DB} = \begin{bmatrix} \cos 2\phi & \sin 2\phi \\ sin\, 2\phi & -cos\, 2\phi \end{bmatrix} \quad (2.20)$$

With ϕ the orientation angle of the dihedral

$$T_{DB} = f_d \begin{bmatrix} |\alpha|^2 & \alpha & 0 \\ \alpha^* & 1 & 0 \\ 0 & 0 & 0 \end{bmatrix} \quad (2.21)$$

With f_d the power contribution of the Double-Bounce scattering and α its scattering ratio.

Fig 2.6 Double-Bounce scattering

2.4.1.3 The Volume scattering

The volume scattering (ex. forest canopy scattering process) is modeled by dipoles oriented in random angles, the scattering matrix and the coherency matrix are giving by [5]:

$$S_v = \begin{bmatrix} cos^2\phi & \frac{1}{2}\sin 2\phi \\ \frac{1}{2} sin\, 2\phi & sin^2\phi \end{bmatrix} \quad (2.22)$$

With ϕ the orientation angle of the dipole.

$$T_v = \frac{f_v}{4}\begin{bmatrix}2 & 0 & 0\\ 0 & 1 & 0\\ 0 & 0 & 1\end{bmatrix} \quad (2.23)$$

With f_d the power contribution of the Volume scattering.

Fig 2.7 Volume scattering

The total coherency matrix of this model is expressed as the sum of the three previous coherencies matrices [5]:

$$T_{tot} = f_s\begin{bmatrix}1 & \beta^* & 0\\ \beta & |\beta|^2 & 0\\ 0 & 0 & 0\end{bmatrix} + f_d\begin{bmatrix}|\alpha|^2 & \alpha & 0\\ \alpha^* & 1 & 0\\ 0 & 0 & 0\end{bmatrix} + \frac{f_v}{4}\begin{bmatrix}2 & 0 & 0\\ 0 & 1 & 0\\ 0 & 0 & 1\end{bmatrix} \quad (2.24)$$

This Three-Component decomposition model has a limited applicability, because the BRAGG scattering is modeled for rough surface backscatter with two complex coefficients under a rigorous roughness constraint [6]. In order to extend the BRAGG scattering applicability the Three-Component decomposition have been modified.

2.4.2 The modified Three-Components decomposition

This decomposition introduces a cross-polarized component generated by the roughness of the underlying surface, the BRAGG scattering component is replaced by an X-BRAGG surface component [5]. This model allows determining the surface roughness extend. The coherency matrix of the BRAGG scattering is replaced by the X-BRAGG scattering coherency matrix presented below [5]:

$$T_{X-B} = f_s \begin{bmatrix} 1 & \beta^* sinc\ 2\delta & 0 \\ \beta^* sinc\ 2\delta & \frac{1}{2}|\beta|^2(1 + sinc\ 4\delta) & 0 \\ 0 & 0 & \frac{1}{2}|\beta|^2(1 - sinc\ 4\delta) \end{bmatrix} \quad (2.25)$$

Where:

- β stands for the roughness effect.
- δ stands for the width of the distribution.
- f_s the power contribution of the X-Bragg component.

As previous, the total coherency matrix of the modified Three-Components decomposition is the sum of the three coherency matrices of each component [5]:

$$T_{tot} = f_s \begin{bmatrix} 1 & \beta^* sinc\ 2\delta & 0 \\ \beta^* sinc\ 2\delta & \frac{1}{2}|\beta|^2(1 + sinc\ 4\delta) & 0 \\ 0 & 0 & \frac{1}{2}|\beta|^2(1 - sinc\ 4\delta) \end{bmatrix} + f_d \begin{bmatrix} |\alpha|^2 & \alpha & 0 \\ \alpha^* & 1 & 0 \\ 0 & 0 & 0 \end{bmatrix} + \frac{f_v}{4} \begin{bmatrix} 2 & 0 & 0 \\ 0 & 1 & 0 \\ 0 & 0 & 1 \end{bmatrix} \quad (2.26)$$

2.5 Conclusion

This chapter was dedicated to the introduction of different approaches for targets decomposition and classification; we have also introduced other strategies in order to describe the surface of a covered area. For the next chapter, we will apply the study using simulated data and operational sensors data.

CHAPTER

3

Results and discussions

3.1 Introduction

As mentioned in the previous chapter, this thesis has for aim the discrimination of soil moisture from agricultural lands; the soil moisture content plays an important role for groundwater recharge, agriculture and soil chemistry. For the case of agriculture, we must point out that not all the water held in soil is available to plants; indeed, plants can absorb soil water, only if its moisture content is optimum for their growth. In the past; different techniques have been studied in order to retrieve soil moisture content (optical and microwave remote sensors), however, and due to their independence of daylight and ability to penetrate cloud cover conditions, microwave remote sensors are much favoured, particularly PolSARs [7] .

The theory held for microwave remote sensing of soil moisture is mostly related to the dielectric constant of the soil. Soil is a mixture of soil particles, air and water, this last has a major dominancy over the dielectric constant, and thus, it is possible to retrieve soil moisture content by measuring the dielectric constant, which is related to the radar backscattering coefficients [8].

In the following, we will present the method used for bare surfaces [11] detection and soil moisture retrieving, we have used simulated and operational sensor data.

3.2 Roughness Angle estimation

In order to obtain accurate estimation of soil moisture, information about the estimation of surface roughness is required, thus in the following we will present the procedure used to retrieve roughness angle [11].

The coherency matrix from (2.26) is the sum of the coherency matrices of an X-BRAGG component, a Double-Bounce component and a Volume component, the roughness angle will be deduced from the X-BRAGG component coherency matrix. We must point out that the method employed is based on modeling the surface under study as a reflection symmetric depolarizer by rotating the X-BRAGG coherency matrix about

an angle β in the plane perpendicular to the scattering plane, consequently, equation (2.25) becomes [9]:

$$T_{X-B} = f_s \begin{bmatrix} C_1 & C_2 sinc\ 2\beta_s & 0 \\ C_2\ sinc\ 2\beta_s & C_3(1 + sinc\ 4\beta_s) & 0 \\ 0 & 0 & C_3(1 - sinc\ 4\beta_s) \end{bmatrix} \quad (3.1)$$

Where:

$$C_1 = |R_{hh} + R_{vv}| \quad C_2 = (R_{hh} + R_{vv})(R_{hh}^{*} - R_{vv}^{*}) \quad C_3 = \frac{1}{2}|R_{hh} - R_{vv}|^2 \quad (3.2)$$

The X-BRAGG coherency matrix is characterized by both a cross-polarized energy and a polarimetric coherence less than one [9]:

$$\gamma_{(hh+vv)(hh-vv)} = \frac{T_{22}}{\sqrt{T_{11}T_{22}}} = \frac{sinc\ 2\beta_s}{\sqrt{\frac{1+sinc\ 4\beta_s}{2}}} \leq 1 \quad (3.3)$$

The polarimetic coherence between the Left-Left and Right-Right circular polarization follows as [9]:

$$\gamma_{(LLRR)} = \frac{T_{22}-T_{33}}{T_{22}+T_{33}} = sinc(4\beta_s) \quad (3.4)$$

The new method mentioned in the introduction consists of substituting the term $sinc(4\beta_s)$ from (3.4) in (3.3) (this substitution is done considering the change of the polarization basis between the *HH/VV* basis and the *LL/RR* basis more details in [2]) we get [11]:

$$sinc(2\beta_s) = \frac{T_{12}}{\sqrt{T_{11}(T_{22}+T_{33})}} \quad (3.5)$$

- ✓ The roughness angle retrieved from equation (3.4) is a function of the diagonal elements (T_{33} and T_{22}) of the matrix (3.1).
- ✓ The roughness angle retrieved from equation (3.5) is a function of the diagonal elements (T_{33} and T_{22}) of the matrix (3.1) in addition to the off-diagonal element (T_{12}).

We conclude that for bare surfaces only, the two retrieved roughness angles from both (3.4) and (3.5) have the same value. Whereas, for a multiple components scattering mechanism (Bare surface + mixed components), the elements of the resulting coherency matrix will be affected by the contributions of the additive components (i.e. Double-Bounce, Volume…etc.), thus, the two retrieved roughness angles will be different.

3.2.1 Simulated dataset

In order to describe in a clearer way the precedent procedure used to discriminate bare surfaces, we will generate a 4-components coherency matrix based on existing models: X-BRAGG, Double-Bounce and Left Helix (the last two are additive components), and a supposed roughness angle. We will add the multiplicative speckle noise by the mean of the Monte Carlo simulations [2].

- For bare surface scattering, as aforementioned the roughness angles are the same, **Fig 3.1** shows the fitting values for a limited roughness angle of ($0° \leq \beta \leq 65°$).

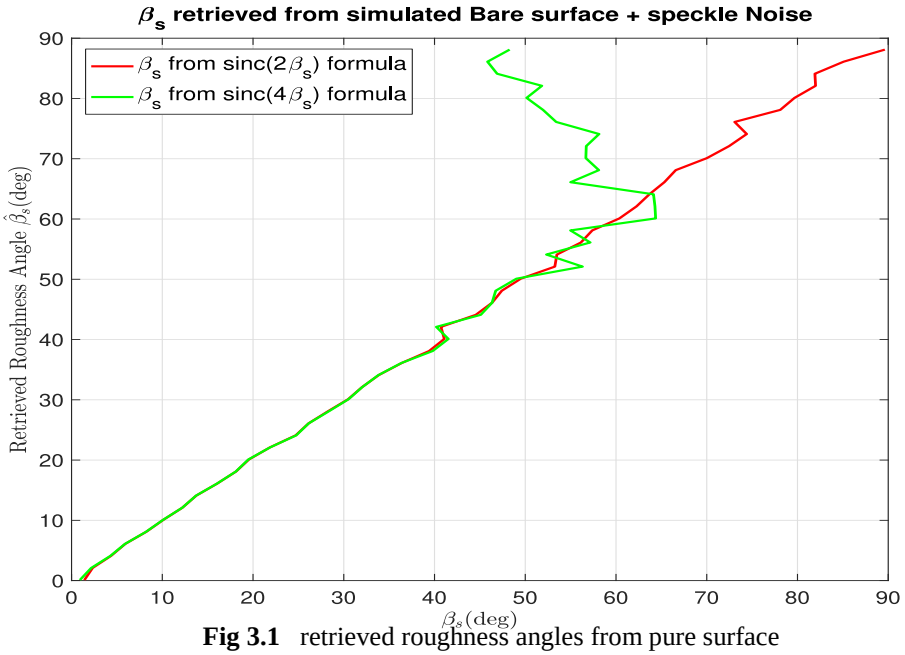

Fig 3.1 retrieved roughness angles from pure surface

Other scenarios for surface scattering (bare surface + additive components) have been simulated, and the results below shows how the two retrieved roughness angles diverge:

- Bare surface + volume.

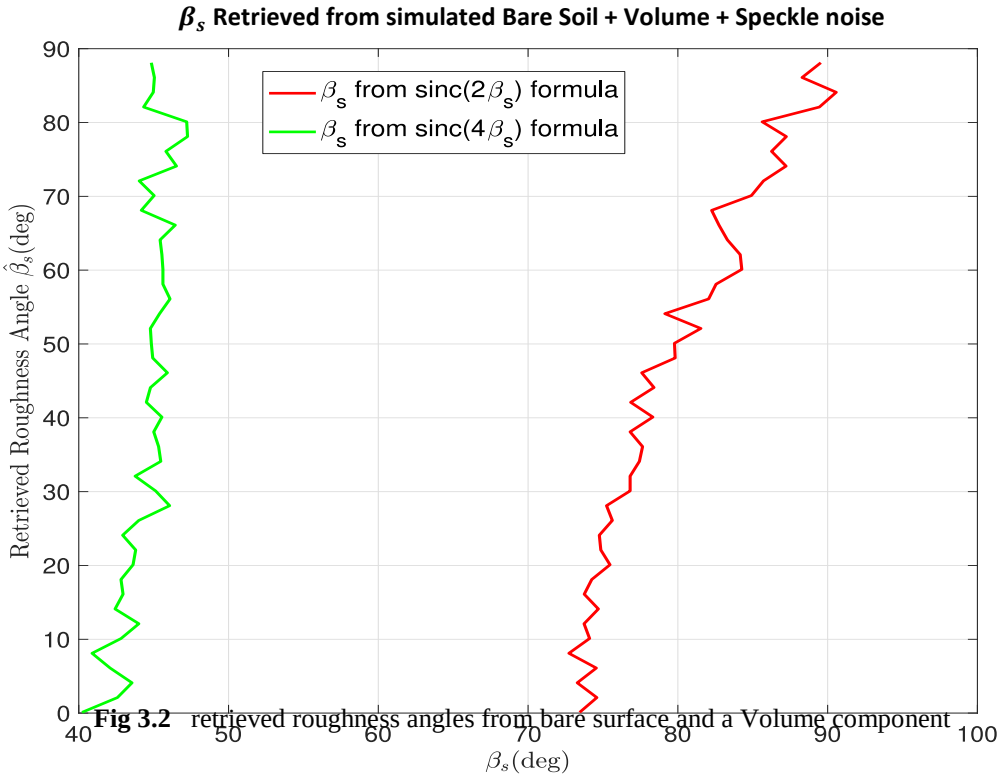

Fig 3.2 retrieved roughness angles from bare surface and a Volume component

- Bare surface + Double-Bounce.

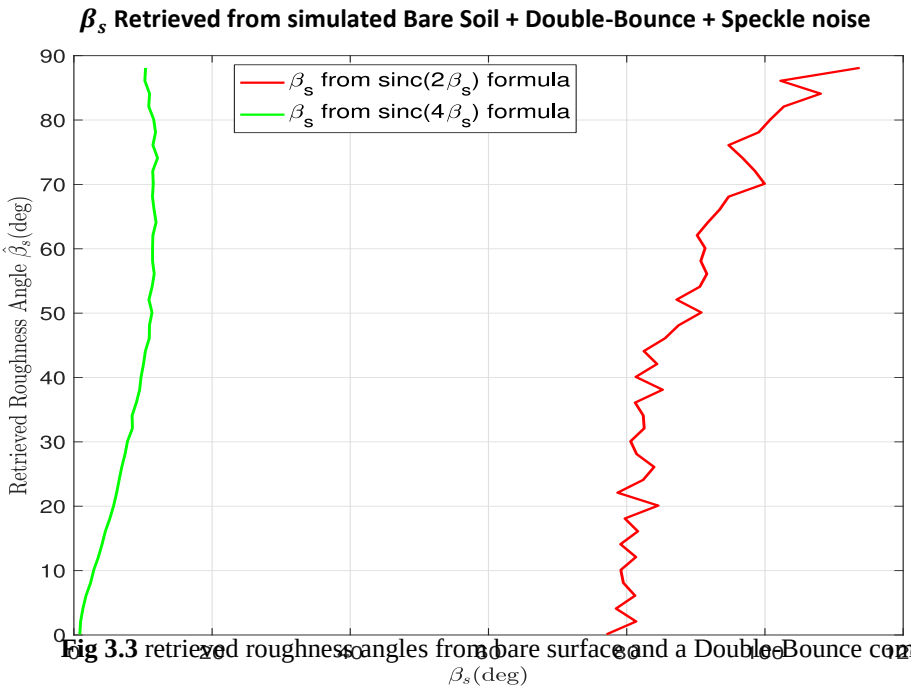

Fig 3.3 retrieved roughness angles from a bare surface and a Double-Bounce component

- Bare surface + Volume + Double-Bounce.

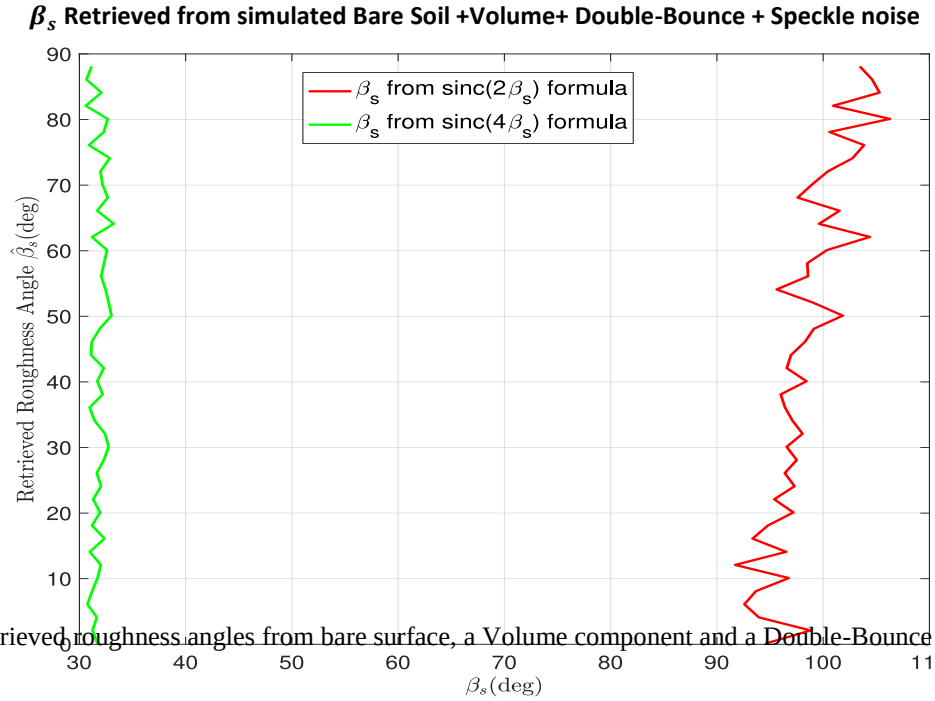

Fig 3.4 retrieved roughness angles from bare surface, a Volume component and a Double-Bounce component

In order to get a global idea about the effect of additive components on the convergence of the two retrieved Roughness Angles, the difference between them have been calculated for each scattering scenario. **Fig 3.5** demonstrate how the additive Volume component affects the distance between the retrieved Roughness Angles.

The difference between the two values increases with the magnitude of the power contributions of the additive component.

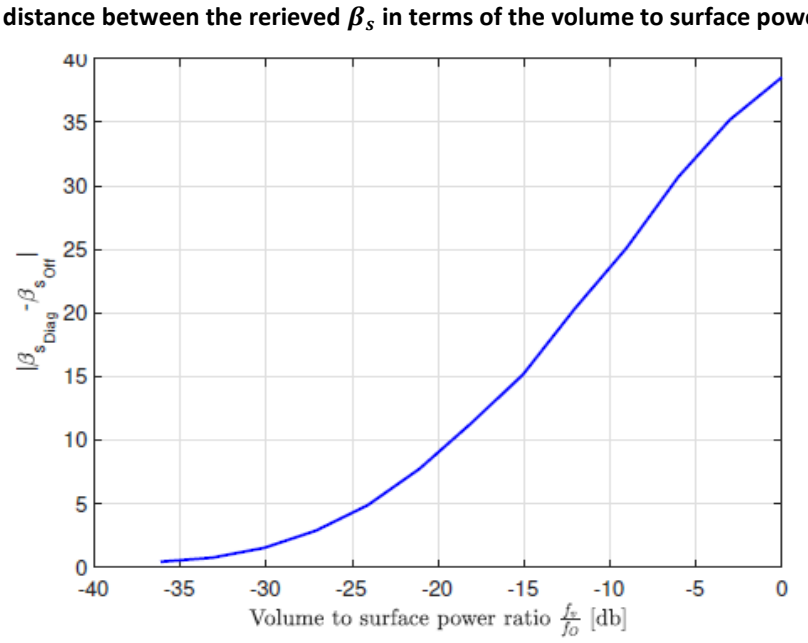

Fig 3.5 effect of additive component on the distance between the Roughness Angles

We may conclude that for an ideal pure scattering surface the distance between the two roughness angles would be null, however, noise is an inevitable parameter thus, a convenient threshold would more likely be used for surface discrimination. For the case of simulated data, the acceptable difference is about $\leq 10°$ i.e. $\frac{f_v}{f_0} \leq -20\ dB$.

3.2.2 Dataset and study area

The operational sensor data are acquired from Oberpfaffenhofen site in Germany, they have been performed using the fully polarimetric L-band (1.3 GHz) with incidence angle ranging from 27° and 55°. **Fig 3.6a** is an optical image of the site which contains different scattering surfaces (Buildings, forests, bare areas).

Fig 3.6a optical image of Oberpfaffenhofen site

The RGB color-coded image of the same site is shown in **Fig 3.6b**

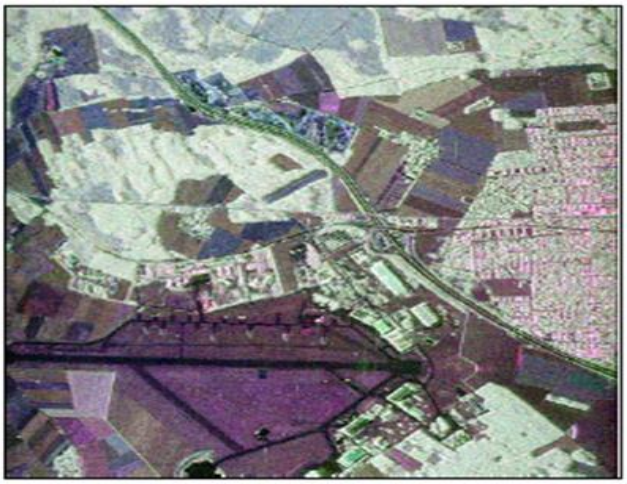

Fig 3.6b RGB color-coded image of Oberpfaffenhofen site

The organizational chart below summarizes the algorithm applied on the data of the study site to discriminate bare soil surfaces and retrieving the moisture content from it.

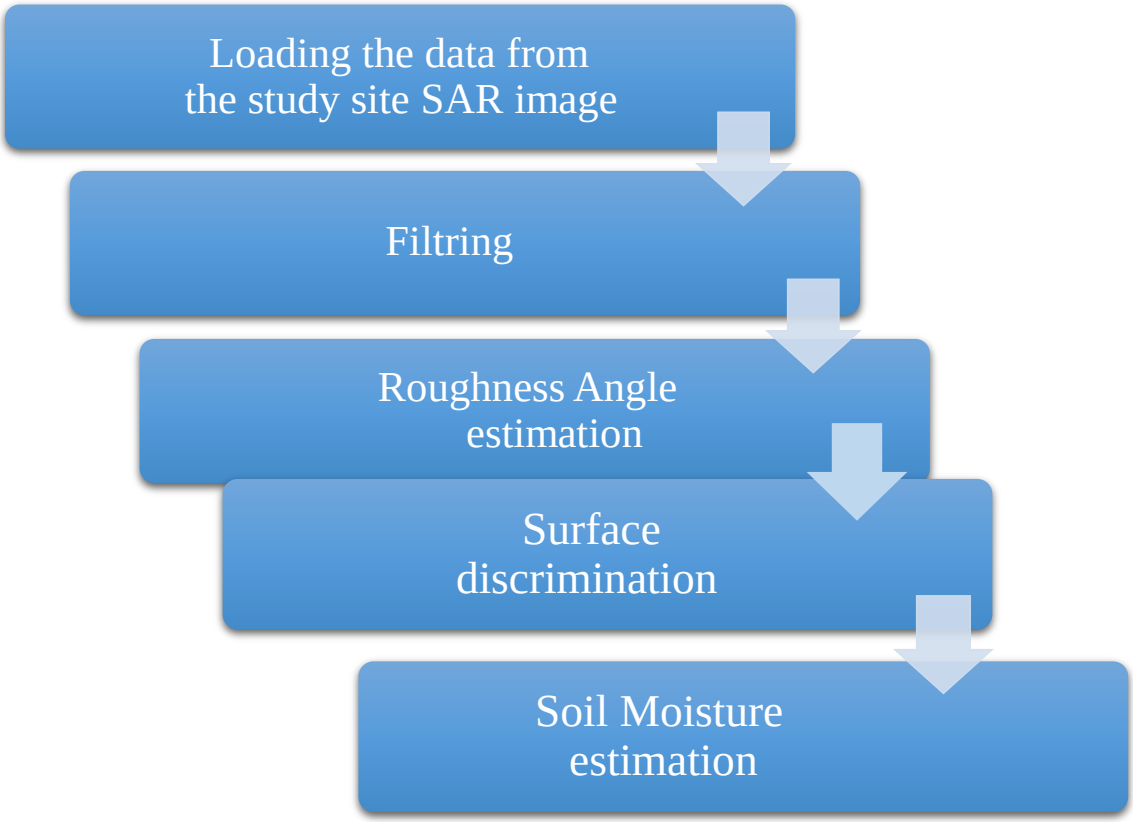

- The results of the SAR image data classification are shown in **Fig 3.7**; the threshold used for bare surface discrimination (the difference between the retrieved) is less than 30°.

Fig 3.7 Classified image of Oberpfaffenhofen site

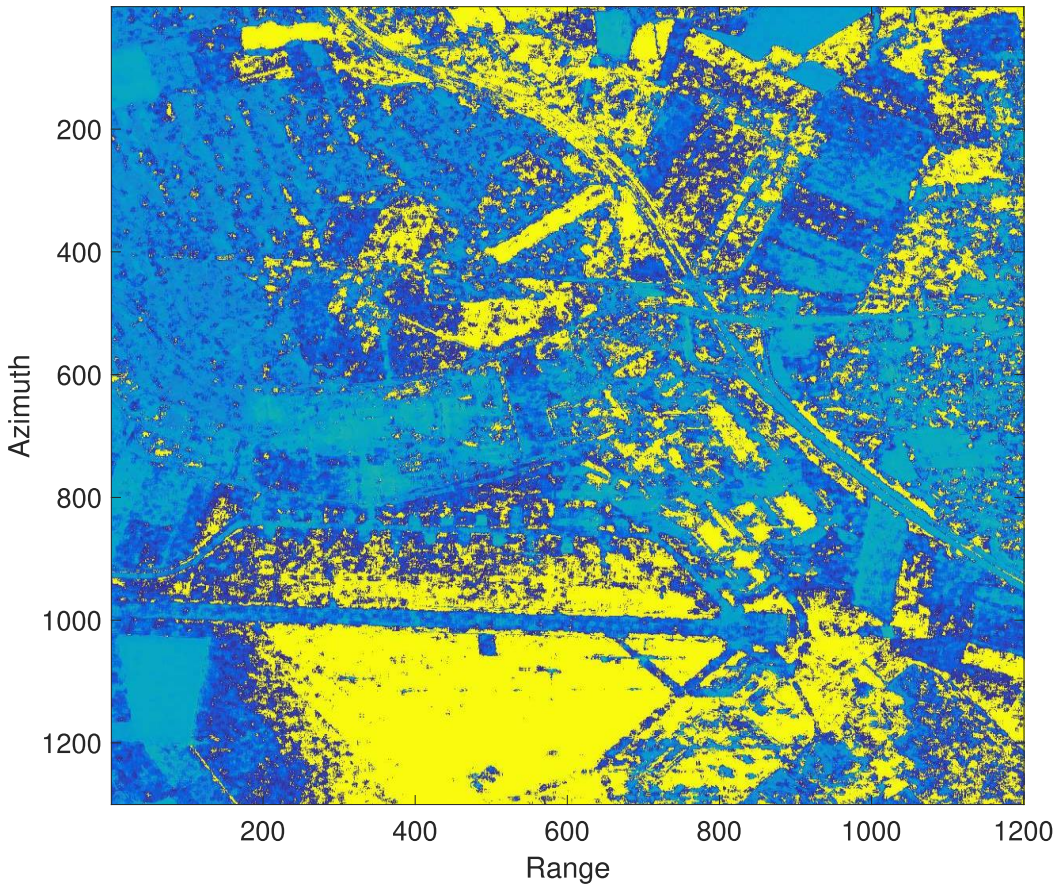

- ✓ The yellow color is associated to Bare Soil class.
- ✓ We can denote that the area around the airport landing strip is yellow colored, by referring to the optical image of the site there is some agricultural lands, which confirms the classification results.
- ✓ In addition to the agricultural lands, the rooftops of the buildings are also classified as Bare Soil.
- ✓ The other areas colored in blue are undefined.

We may conclude that the classification using that threshold has acceptable results.

3.3 Soil-Moisture estimation

After the discrimination of the bare surface areas by retrieving the roughness angles, we will estimate the moisture content of the underlying ground by determining the dielectric properties of the soil, which are directly linked to the surface scattering components.

In this case, a simple inversion of the roughness real ratio β will give the real part of the dielectric constant of the soil ε_s. The obtained estimations are then converted into volumetric soil moisture, by the mean of a polynomial relation given as follows [10]:

$$MC = 0.0004\,{\varepsilon_s}^3 + 0.055\,{\varepsilon_s}^2 + 2.92\,\varepsilon_s - 5.3 \qquad (3.6)$$

Conclusion

The aim of the present work is to estimate the soil moisture content in bare soil surfaces, we first needed to discriminate the soil surface by retrieving the roughness angle, for this purpose a new method using the X-Bragg component was applied to the data extracted from the SAR image.

The method was first applied on simulated data that englobed different scattering mechanisms, the results confirmed the hypotheses put for the two formulas used to retrieve the roughness angle; in addition, the simulation allowed us to determine a threshold that we will use for the real sensor data.

The method was then applied on real sensor data of a study site, the surface discrimination was established by respecting a fixed threshold that enabled us to have an acceptable margin. By referring to the optical image of the site, the results could be verified.

We may conclude that the method used is very efficient for the discrimination of bare surfaces; thus, the soil moisture will be retrieved.

References

[1] E. Pottier. *SAR POLARIMETRY Basics Concepts, Advanced Concepts and Applications. 2013.*

[2] J-S. Lee, E. Pottier. *Polarimetric Radar Imaging: from basics to applications*.2009

[3] W. Bu-Chin. *Digital Signal Processing Techniques And Applications In Radar Image Processing: A JOHN WILEY & SONS, 2008*.

[4] C. Lopez-Martinez, L. Ferro-Famil, E. Pottier. *Tutorial on polarimetric SAR*. January 2005.

[5] I. Hajnsek, T. Jagdhuber, K. Papathanassiou. *Potential of estimating soil moisture under vegetation cover by means of PolSAR.* 2009

[6] J. Yin, J. Yang, Z. Zhou, J. Song. *The Extended Bragg Scattering Model-Based Method for Ship and Oil-Spill Observation Using Compact Polarimetric SAR.* 2014.

[7] B. Barett, E. Dwyer, P. Whelan. *Soil Moisture Retrieval from Active Spaceborne Microwave Observations: An Evaluation of Current Techniques. Remote sensing. 7 july 2009*

[8] F.T. Ulaby, C. Elachi. *Radar Polarimetry for Geoscience Applications. Artech House: Norwood, MA, USA, 1990*

[9] I. Hajnsek, E. Pottier, R. Cloude. *Inversion of Surface Parameters From Polarimetric SAR. 2003-04-04*

[10] G. C. Topp, J. L. Davis, and A. P. Annan. "*Electromagnetic determination of soil water content: Measurements in coaxial transmission lines," Water Resour. Res., vol. 16, no. 3, pp. 574–582, 1980.*

[11] S. Tahraoui, M. Ouarzeddine. *A New Approach for rough Surfaces Detection Based on extended Bragg covariance matrix model*.2020-04-16